Scientific Reports

https://doi.org/10.1038/s41598-026-42740-4

Article in Press

Understanding tens of thousands of pockmarks and domes using machine learning (Gulf of Lions, NW Mediterranean Sea)

Received: 12 December 2025

Accepted: 27 February 2026

Published online: 24 March 2026

Cite this article as: Lion A., Bassetti M., Berné S. *et al.* Understanding tens of thousands of pockmarks and domes using machine learning (Gulf of Lions, NW Mediterranean Sea). *Sci Rep* (2026). https://doi.org/10.1038/s41598-026-42740-4

André Lion, Maria-Angela Bassetti, Serge Berné & Romain Jatiault

Understanding tens of thousands of pockmarks and domes using machine learning (Gulf of Lions, NW Mediterranean Sea)

Authors

Lion André, Bassetti Maria-Angela, Berné Serge, Jatiault Romain

All authors are affiliated with the University of Perpignan, Perpignan, France, Centre de Formation et de Recherche sur les Environnements Méditerranéens, UMR 5110 CNRS.

Corresponding author: André Lion

Research funding

This research did receive funding.

André Lion received funding from French Ministry of Higher Education, Research and Space.

André Lion received funding from Office Français de la Biodiversité.

Abstract

A broad spectrum of seabed deformation structures, including pockmarks and domes, related to various processes, have been observed on continental margins worldwide. This study provides the first regional-scale inventory and quantitative characterization of pockmarks and domes potentially linked to subsurface fluid-escape processes on the continental shelf and upper slope in the Gulf of Lions (NW Mediterranean). Using high-resolution multibeam bathymetry and seismic reflection data, approximately 29,000 pockmarks and domes were identified. Morphometric and seismic analyses reveal distinct groups that differ in size, shape, and spatial organization. Among them a widespread population of domes rooted on the Holocene Maximum Flooding Surface, which represent ~85% of the occurrences. The remaining 15% are pockmarks, divided into five main subtypes. Spatial association of domes and pockmarks suggests a genetic relationship between dome formation and subsequent collapse (pockmarks). Machine learning–based spatial modeling, extends the estimated total to ~80,000 between 10 and 1000 m water depth, including zones not covered by swath-bathymetric surveys. Among various controlling factors, sediment thickness, water depth, and grain-size variability exert primary controls on the distribution of pockmarks and domes. These results demonstrate that seabed deformations in the Gulf of Lions are spatially organized, reflecting the interplay between fluid-related processes, stratigraphic architecture, and sediment properties.

Keywords

Pockmarks

Domes

Gulf of Lions – northwest Mediterranean Sea

Machine learning

Cold seeps

Maximum Flooding Surface

I. Introduction

Subsurface sediment mobilization, as described by Van Rensbergen et al. [1], encompasses the suite of processes by which sediments undergo remobilization, displacement, or internal deformation in response to changes in pore-fluid pressure, mechanical properties, or stratigraphic architecture. Although these mechanisms occur within the shallow subsurface, their expression frequently reaches the seafloor, giving rise to seabed deformation structures (SDS). These geomorphological features occur across a wide variety of physiographic settings, including continental shelves, slopes, abyssal plains, and inland seas, they represent the seafloor imprint of subsurface dynamics [1,2].

While SDS may result from non-fluid processes such as mechanical contrasts, differential compaction or sediment loading, most of them are associated with the ascent of fluidized sediments within shallow environments [1] and fall into the category of cold seeps [3]. Processes contributing to seep-related deformation include gas generation, groundwater discharge, sediment compaction, brine expulsion, hydrocarbon migration and gas hydrate destabilization [4–6]. Methane, often exceeding 90 percent of the gaseous phase in natural seeps [7], may originate through microbial degradation of organic matter [8] or thermal cracking at depth [9]. When overpressure reaches critical thresholds, fluids and gases migrate upward, producing typical seabed expressions detectable by geophysical methods. Among SDS, pockmarks constitute the most widely documented type [10,11], including in the Mediterranean Sea [12,13]. Positive relief such as sedimentary domes, mud volcanoes, and mounds have also been documented [14–17].

Identifying and distinguishing SDS requires the integration of multiple datasets [18,19]. Multibeam bathymetry resolves the fine-scale morphology of the seafloor, while high-resolution seismic reflection data reveal vertical conduits and disturbed intervals such as acoustic blanking zones, enhanced reflectors, and gas chimneys [20].

The Gulf of Lions (GoL) in the northwestern Mediterranean Sea hosts several conditions favorable to a wide range of SDS. These include thick Quaternary sediment accumulations, stratigraphic traps, and both biogenic and thermogenic gas-bearing strata [21,22]. Additionally, evidence of fresh or brackish water escape has been described in the coastal zone. They correspond to the marine extent of karstic aquifers, possibly active during the Messinian drawdown [23], and potentially still active nowadays [24]. Despite this context, the regional distribution, diversity, and origins of SDS in the GoL have remained poorly constrained. Recent high-resolution industrial geophysical surveys, combined with existing academic datasets, now enable a comprehensive examination of SDS across the shelf and upper slope. In light of the newly available dataset, the overarching questions of this study are:

What are the extent, diversity, and spatial distribution of SDS in the Gulf of Lions, and what factors control their occurrence?

To address these questions, the study pursues three specific objectives:

1. Detection and classification – Identify and classify SDS such as pockmarks and domes, using high-resolution multibeam bathymetry and seismic data.
2. Quantification and mapping – Determine the abundance, size-frequency distribution, and spatial patterns of the SDS, and evaluate their relationship with seafloor and subsurface lithologies.
3. Predictive modeling – Obtain a better understanding of the factors controlling SDS repartition through a basin-wide map across the Gulf of Lions shelf and upper slope (0–1000 m) and interpolation of SDS densities using machine learning.

Through the combined use of morphometric analysis, geophysical imaging, and predictive modelling, this study provides the first integrated assessment of SDS in the Gulf of Lions and improves regional understanding of subsurface sediment mobilization and fluid-related processes on continental shelves.

II. Study Area

The Gulf of Lions is a wide (up to 70 km), gently dipping (<1°) continental shelf (Fig. 1-a), with the shelf break located between 120 and 160 m water depth. The margin is incised by numerous submarine canyons, shaped during the post-Messinian reorganization of the continental edge following the Messinian salinity crisis [25,26]. Above the Messinian Erosion Surface, a Plio-Quaternary sedimentary infill up to 2000 m thick accumulated, driven by high sediment supply from the Rhône River and accommodation created by Messinian subaerial erosion [26].

A high subsidence rate at the shelf edge (~250 m/My; [27]) enabled preservation of multiple stacked forced-regressive wedges thickening basinward. The uppermost sequence corresponds to the last 100 ka glacio-eustatic cycle and includes a series of regressive units formed during Marine Isotope Stage (MIS) 3–2 sea-level fall. These are overlain by a polygenic erosion surface [28,29], locally incised on the inner shelf by paleo-valleys [30]. On the outer shelf, this regressive system is capped by transgressive sand bodies (<10 m thick), reworking MIS 2 shorefaces and shelf-edge deltas [29,31,32].

During the last post-glacial sea-level rise (20-7 ka cal. BP), the landward migration of depocenters such as estuary-mouths formed shoal retreat massifs as defined by Swift et al. [33,34]. They are erosion-resistant bodies composed of relict sandy deposits sometimes draped by a thin layer (centimeters to meters) of mud, they form a positive-relief easily recognized on bathymetric maps [31,35].

In mid-shelf settings (35–80 m water depth), a sigmoidal transgressive prism up to 40 m thick overlies the regressive to early transgressive deposits (Fig. 1-b and e). This unit is primarily composed of fine-grained sediments advected from the Rhône, forming a well-defined mud belt [36]. It includes late Pleistocene, early Holocene (ca. 20 ka to ~7.5 ka cal BP) deposits, occasionally arranged in backstepping parasequences [35], overlain by a regressive mid- to late Holocene unit (~7.5 ka cal BP to present). The surface separating transgressive deposits (below) from regressive deposits (above) is the Maximum Flooding Surface (MFS). On seismic

profiles, this surface is a regionally correlable high-amplitude reflection (Fig. 1-b and e), sometimes marked by faint downlap seismic terminations. It is dated at approximatively 7.5 ka cal BP in the central Gulf of Lions [36]. This surface is visible and described in sediment cores at two sites in the GoL, where it corresponds to coarser intervals overlain by clayey deposits [35 (their figure 9),36 (their figure 4)]. The reason is that MFSs correspond to the period when sediment sources (estuaries) are located farther landward, which favors erosion and winnowing of the fine fraction, resulting in the formation of a condensed interval (see [37] for a detailed review of processes and products). This lag interval is eventually buried by muds when delta progradation resumes.

Between 0 and ca 90 m water depth, surface sediments exhibit a general fining-seaward trend, from nearshore well-sorted sands to offshore silty clays [38], with local enrichments in coarser material near river mouths [39]. The Rhône currently supplies ~90% of the suspended sediment load to the shelf, with <5% of this flux corresponding to sand [40].

Although GoL has been extensively studied, few fluid-related SDS were observed on the seafloor within the study area and no comprehensive inventory of SDS exists to date. Thus, their formation mechanisms, activity status, and temporal evolution remain insufficiently constrained. On the upper slope, between the Bourcart and Hérault canyons (BC and HC in Fig. 1-a), dense alignments of pockmarks have been interpreted as resulting from active or past methane seepage processes [41,42].

III. Materials and Methods

A. Data set

This study is based on a multi-source geophysical dataset acquired during several oceanographic cruises conducted across the Gulf of Lions. The mapping process relies on Digital Elevation Models (DEMs) derived from multibeam bathymetric data (Fig. 1-a), acquired between 1995 and 2024 for academic, environmental, or industrial purposes. The chronology of various surveys, as well as the technical specifications of the multibeam echosounder (MBES) acquisition systems and data ownerships are summarized in Supplementary Table 1.

Data preparation

Residual elevation was derived by subtracting a smoothed DEM from the original to isolate local morphological structures [43]. The regional trend surface was generated using the *Resampling Filter* [44]. This method first upscales the grid via area-weighted averaging, with a target resolution of 100 meters, then downscales it to the original resolution using spline interpolation. This two-steps approach effectively acts as a low-pass filter and provides a computationally efficient method for separating topographic components based on their scale. Processing routines were applied when needed to reduce artifacts including sound velocity anomalies, edge effects, and acquisition noise. The primary method employed was a two-dimensional Fast Fourier Transform (2D FFT), allowing the transformation of residual elevation grids into the k-space (wavenumber domain). In this domain, noise and artifacts,

often related to acquisition, can easily be attenuated using a filtering function. The isolated artifacts filtered in k-space are then transformed back into the spatial domain and subtracted from both the residual elevation and the original bathymetric grids. Median filtering was then applied only to DEMs where noise-induced artifacts were not resolved by frequency-domain processing. This processing approach was preferred due to its effectiveness in suppressing acquisition-related noise patterns without affecting geological structures or having to reprocess raw data, often unavailable.

In addition, residual elevation mapping and machine learning results are completed by interpretation of 2D high-resolution seismic reflection profiles to support the hypothesis and interpretations. The Gulf of Lions has been extensively surveyed during numerous academic and industrial geophysical cruises, with seismic data coverage concentrated in the areas where DEMs were produced (see Supplementary Table 1). Data has been acquired with sparker, chirp, and sub-bottom profiler systems. However, the small dimensions of SDS often complicates their detection, either because the vertical resolution of seismic acquisition is insufficient or because surveys do not directly cross SDS.

B. Mapping and interpolation

A supervised machine learning approach was applied to predict the spatial distribution of SDS where high resolution bathymetry is unavailable. Data processing and the following modelling steps are summarized in a schematic overview to facilitate understanding of the methodology (Fig. 2-a). Input data are structured using Hexagonal Hierarchical Geospatial Indexing (H3) with cells of ~0.7 km² (resolution 8 according to H3 resolution system) [45], providing a uniform spatial indexing framework (Supplementary Figure 2). Within each H3 cell, the number of identified SDS was counted for each type. Cells covered by the merged DEM dataset were used for model training and validation (green cells in Supplementary Figure 2). Only cells with complete DEM coverage (green) were included in the dome prediction model, whereas the pockmark prediction model incorporated both fully and partially covered cells (green and red) to integrate a significant number of mapped SDS.

The five available **predictor variables** to perform the prediction include slope gradient, thickness of the last sedimentary sequence (S6 as described by Jouet [46]), water depth [47], as well as grain-size distribution for clay, sand, and silt. Grain-size distribution was obtained by natural neighbor-interpolation of the surface sample (grabs and cores) from the Gulf of Lions compilation [48]. For each variable, zonal statistics, namely mean, median, standard deviation, minimum, and maximum value were calculated within each H3 cell, resulting in a total of 30 input variables. Area of each cell was also added to correct the potential bias caused by partially mapped cells.

The **model targets** are the counts of deformations for each class within each cell. The dataset was randomly split into training (80 %) and test (20 %). The model used is a Light Gradient Boosting Machine (LightGBM) [49], implemented within a multi-output regression framework predicting all target variables in a single run.

Hyperparameter optimization was performed using randomized search with 30 iterations and three-fold cross-validation. The best-performing parameters identified were: learning rate = 0.09, maximum tree depth = 66, and number of estimators = 300.

Feature importance was evaluated using SHAP (SHapley Additive exPlanations) values [50]. SHAP assigns a score to each input variable, based on its contribution to the model's predictions, allowing a clear and consistent interpretation of which parameters most influence the output. Mean absolute SHAP values were used to rank variables and identify the main controls on the distribution of domes and pockmarks.

Model performance was evaluated using the coefficient of determination (R^2) and root mean square error (RMSE) on both training and validation sets. Evaluation results are summarized in Fig. 2-b. These performance metrics indicate high predictive performance for the Domes and Type B pockmarks classes. Lower performances in other classes have been attributed to both the low representation of the class, especially spiky pockmarks, and the fact that this study only uses a limited number of predictors, leaving some unaccounted for.

IV. Results

A. Identification of seabed structures

1. Domes

Domes, are positive-relief SDS that appear as rounded mounds on the seafloor. These structures are observed exclusively on the continental shelf, at water depths ranging from 60 to 125 meters. Their typical dimensions are approximately 1 meter in height and around 100 meters in diameter (Fig. 3-a). While dome size may vary from 0.30 to 1.2 meter in height and 80 to 130 meters in diameter, size seems consistent between neighboring domes. However certain areas are dominated by smaller domes (less than 60 m in diameter and 0.60 m high), whereas others are dominated by larger structures. Morphologically, all domes exhibit a high degree of circularity with minimal elongation and display a random spatial distribution within the field.

In seismic sections, initial deformations are anchored on a ***regionally correlable reflection*** identified as the MFS [35,36] (Fig. 1-d and 5-a). Geophysical analysis using instantaneous seismic attributes [51] reveals the presence of high-strength reflections at the base of the domes (Fig. 5-b). Domes, regardless of their size, are consistently associated with "bright spots" characterized by higher reflection strength. These bright spots coincide with high-frequency attenuations of the underlying reflections (Fig. 5-c) and exhibit a local phase shift, resulting in an apparent negative polarity of the seismic signal (Fig. 5-d and e).

2. Pockmarks

Based on the morphometric parameters derived from the residual elevation model, four subtypes of pockmarks were distinguished (Fig. 3).

Type A pockmarks are the largest SDS, with diameters exceeding 150 meters and occurring on interfluves between submarine canyons, at water depths ranging from 120 to 520 meters. Individual structures can reach up to 500 meters in diameter and 10 meters in depth (Fig. 3-b). These pockmarks are often aligned along preferential axes, most commonly NW–SE, parallel to the canyon axis. Type A pockmarks tend to form clusters, where they present a regular spacing of 200–300 meters. A slight asymmetry is typically observed, with the steepest flank facing southward. In seismic section, Type A pockmarks are associated with large oblique V-shaped chimneys (Fig. 4), are anchored deep in the substratum and can affect multiple sequences successively (up to MIS 8a sequence boundary).

Type B pockmarks are medium-sized depressions, with diameters ranging from 50 to 150 meters and depths around 1 meter. They are represented in the widest range of environments, occurring across both the shelf and the continental slope, from 70 to 750 meters water depth. These structures do not exhibit any consistent spatial arrangement, although spacing is often regular within the 100- to 200-meter range. Unlike Type A pockmarks, they do not present any asymmetry. On seismic profiles, Type B pockmarks are associated with small chimneys, they are typically anchored shallow in the sediment pile (Fig. 4). They rarely affect more than one consecutive depositional sequence. Smaller Type B pockmarks are frequently found nested within larger Type A pockmarks (Fig. 3-b).

Type C pockmarks correspond to the smallest depressions, they are typically found between 15- and 35-meters water depth. They have irregular distribution, sometimes less than a meter apart, and show no consistent pattern in spatial organization (Fig. 3-c). Depths range from 10 to 30 centimeters, and diameters from 5 to 15 meters. In cross-section, Type C pockmarks are symmetrical and show no preferential orientation. The small scale of Type C pockmarks makes their internal structure hardly distinguishable in seismic section (Fig. 1-c).

Type D pockmarks are irregularly shaped depressions occurring exclusively on the shelf, particularly on the mid- to outer shelf in the central Gulf of Lions, between 60- and 95- meters water depth. These structures vary widely in shape and size, ranging from 100 to 500 meters in diameter, while maximal depth consistently approximates 1 meter (Fig. 3-d). Toward the coast, they are circular to slightly elongated; seaward, they become patchier and sinuous, with elongated forms often aligned NW–SE. Their spacing is highly irregular, and no organized pattern is observed. Similarly to Type B pockmarks, Type D pockmarks are anchored shallow in seismic section (no deeper than the MFS; Fig. 1-f). They do not display any chimney but are rooted on the MFS, giving them a characteristic asymmetry with a steep flank shoreward, evolving to a flat bottom seaward (Fig. 3-d and 1-f).

Beside these main morphological types, a set of rare morphologies such as **spiky pockmarks** are morphologically similar to Type B pockmarks, but they are characterized by a central conical spike (Fig. 3-e). The central spike rises approximately 20 centimeters above the seafloor and measures about 10 meters in diameter. They are often isolated or aligned along axes parallel to shoal retreat massifs. Neither the depression nor the central spike display asymmetry or elongation.

B. Distribution of seafloor deformation structures and Machine Learning Interpolation

A total of **28,572 sediment deformation structures** were mapped, comprising approximately 86% domes and 14% pockmarks (Fig. 6). Although local distributions can appear random, the large-scale mapping and machine learning predictions reveal spatially organized patterns, with marked clustering and spatial segregation between pockmarks and domes (Fig. 6). More precisely, domes are observed primarily in the distal part of the Rhône mud belt (Fig. 1-b and d) while pockmarks are found in distinct areas depending on their morphological type:

- Type A pockmarks occur on canyon interfluves.
- Type B pockmarks are ubiquitous and are often found in association with other SDS, especially with domes and Type A pockmarks.
- Type C pockmarks are located on the Infralittoral Prograding Wedge (IPW) [52].
- Type D pockmarks form a centrally located patch on the continental shelf.
- Spiky pockmarks are observed in proximity to shoal retreat massifs, associated with the Rhône and Lacaze-Duthiers sectors.

In order to confirm the correlation between the pockmark types, slope gradient, water depth and the sedimentary environments, a machine learning model was applied (Fig. 7), yielding an estimated total of approximately 55000 predicted pockmarks and domes over the entire Gulf of Lions (including zones where no DEM is available). The SHapley Additive exPlanations (SHAP) analysis demonstrates that the relative influence and direction of predictor variables vary among morphological classes (Fig. 8).

For **domes** (Fig. 8-a), the minimum thickness of the last sedimentary sequence ($Thickness^{S6}_{min}$) exerts the dominant control on model output (mean |SHAP| ≈ 3.7). Low $Thickness^{S6}_{min}$ values (blue) correspond to strongly negative impacts (–5 to –7), whereas high values (red) produce large positive effects (up to +10), indicating that thicker uppermost sedimentary layer favor dome formation and preservation. Maximum depth ($Depth_{max}$) and clay standard deviation ($Clay_{std}$) follow in importance (≈ 1.7 and 1.6, respectively). Low $Clay_{std}$ values (blue), reflecting more homogeneous and fine-grained deposits, are consistently associated with higher predicted probabilities. Minimum clay content ($Clay_{min}$) and maximum S6 thickness ($Thickness^{S6}_{max}$) have smaller but distinct effects. These relationships reinforce the interpretation that domes develop preferentially at the distal margin of the Rhône mud belt, where fine-grained, clay-rich sediments thin toward the outer shelf. In addition to the regional patterns identified by the model, hand mapping shows that areas containing smaller domes tend to display a higher spatial density, whereas regions dominated by larger domes exhibit lower spatial density.

For **Type A pockmarks** (Fig. 8-b), water depth variables dominate the prediction. $Depth_{max}$ shows the highest contribution (mean |SHAP| ≈ 0.35), followed by $Thickness^{S6}_{min}$, $Thickness^{S6}_{std}$, maximum slope gradient ($Slope_{max}$), and minimum depth ($Depth_{min}$). High $Depth_{max}$ values (red) are associated with positive SHAP impacts, suggesting that this

pockmark subtype preferentially develops in deeper settings, whereas slope-related variables exert a more moderate influence (|SHAP| < 0.2).

Type B pockmarks (Fig. 8-c) also exhibit a strong bathymetric control, with $Depth_{max}$ and $Depth_{min}$ showing the largest contributions (|SHAP| ≈ 4–5). Secondary predictors include median S6 thickness ($Thickness^{S6}_{med}$), maximum slope gradient ($Slope_{max}$), and mean slope gradient ($Slope_{mean}$) (|SHAP| ≈ 1.5–2). High depth and slope gradient values (red) correspond to positive SHAP effects, indicating that Type A and Type B pockmarks occur preferentially in deeper and steeper setting, as previously observed on canyons interfluves.

For **Type C pockmarks** (Fig. 8-d), model sensitivity is lower overall (|SHAP| ≤ 0.04). The main contributors—minimum depth ($Depth_{min}$), mean clay content ($Clay_{mean}$), mean depth ($Depth_{mean}$), sand standard deviation ($Sand_{std}$), and median clay content ($Clay_{med}$)—suggest that this subtype forms in shallow, clay-rich environments with moderate lithological variability. High $Depth_{min}$ and $Depth_{mean}$ values (red) are linked to positive SHAP effects, implying greater occurrence like those found in fine-grained sediments.

Type D pockmarks (Fig. 8-e) are primarily controlled by sediment lithology. Maximum sand content ($Sand_{max}$) yields the largest contribution (mean |SHAP| ≈ 0.10), followed by minimum and mean silt content ($Silt_{min}$, $Silt_{mean}$), and minimum and maximum clay content ($Clay_{min}$, $Clay_{max}$) (≈ 0.05–0.08). High $Sand_{max}$ values (red) are associated with positive SHAP effects, whereas high $Clay_{max}$ values (red) reduce the predicted probability, indicating that Type D pockmarks are more frequent in coarser, sand-rich substrates.

Spiky pockmarks (Fig. 8-f) display the weakest overall SHAP values (|SHAP| ≤ 0.008), which reflects their weak representation (Fig. 6-b). The main predictors—maximum S6 thickness ($Thickness^{S6}_{max}$), maximum silt content ($Silt_{max}$), minimum sand content ($Sand_{min}$), minimum silt content ($Silt_{min}$), and mean clay content ($Clay_{mean}$)—exhibit subtle but consistent effects. High $Thickness^{S6}_{max}$ and $Silt_{max}$ values (red) slightly increase model output, whereas low sand and clay values (blue) reduce it. This suggests that spiky pockmarks might occur in association with sandy sediments within the most recent sedimentary sequence.

Overall, these results also indicate that pockmark distribution is likely tied to broader settings rather than surface sedimentary variability. It is also important to note that the model was constrained to a limited set of surficial parameters, leaving several potential predictors unaccounted for.

V. Discussion

The spatial distribution, morphology, and variability of pockmarks and domes identified on the Gulf of Lions shelf correlate with grain-size distribution, water depth, and slope gradient, as revealed by geomorphological mapping and modeling. Nonetheless, formation mechanisms cannot be directly resolved from mapping and modeling. The following synthesis integrates geomorphological, sedimentological, and seismic evidences to interpret the processes and controlling factors involved.

Although the nature of the **domes** (Fig. 3-a) observed in the Gulf of Lions remains to be deciphered, machine learning analyses along with seismic data support some hypothesis on their origin and formation processes. The most obvious observation is their spatial distribution, since domes appear mostly along the distal pinch-out of the Rhône mud belt. We suppose that the seaward thinning of the mud belt (made of fine-grained sediments) allows for two key factors in dome formation: an horizontal impermeable layer of relatively small thickness [14]. Methane seepage appears to be the most plausible driving process, as it was already mentioned in previous studies around the world (see the compilation by Barry et al. [14]. In the Gulf of Lions, the migrating fluids possibly accumulate within the coarse and permeable MFS, while the overlying fine-grained sediments seal this temporary reservoir. Progressive pressurization might drive the deformation of the overlying sediments, forming dome-shaped seabed structures. This hypothesis is further supported by the presence of acoustic indicators such as amplitude anomalies, high amplitude attenuation, phase rotation and negative apparent polarity [51] at the base of domes in seismic data, that might relate to gas occurrence (Fig. 5). Other processes could intertwine in the generation of domes, such as confined groundwater discharge, lateral sediment loading, or differential compaction, which all may contribute to overpressure development and/or sediment deformation [1]. Biological activity associated or not with methane oxidation may further enhance sediment cohesion and structural stability. Moreover, sediment intrusion processes, whereby material is fluidized and transported upward through migrating fluids, may contribute to the development of domes [53].

Given enough time and the right conditions, under sustained or increasing overpressure, domes formed within Holocene sediments of the Rhône mud belt may collapse and evolve into pockmarks. This dome-to-pockmarks evolution will be further discussed along with Type B pockmarks.

Previous studies in the Gulf of Lions identified **Type A pockmarks (Fig. 3-b)** and emphasized the role of sea-level fluctuations as the main triggering mechanisms of alternating phases of pressure buildup, fluid migration, and seepage [41,42]. This cyclicity was linked to 100-kyr eustatic cycles, during which repeated transgressive–regressive events modulated sediment loading and pore-pressure variations within the underlying strata. Regarding the structural deformation of sediments associated with pockmark formation, explanations remain inconclusive. Gay et al. [41] proposed that doming precede collapse, whereas Riboulot et al. [42] suggested that venting is not necessarily preceded by mechanical doming. The doming hypothesis [41] is supported by the conical upward-widening morphology of pockmarks observed in cross-section, interpreted as evidence of progressive upward deformation prior to failure. However, alternative explanations attribute this conical geometry to oblique growth controlled by hydrodynamic processes rather than subsurface doming [42].

The co-existence of **Type B pockmarks** (Fig. 3-b) and domes on the shelf (Fig. 3-f), as well as their similarity in diameter, suggest a dome-to-pockmark evolution as proposed by Vaknin et al. [6]. According to these authors, domes form first as a result of upward sediment deformation; once critical mechanical thresholds are exceeded, depending on the elastic or brittle properties of the sediment package [54], collapse occurs, producing a negative-relief depression. This interpretation aligns with observations from several continental margins

where dome-to-pockmark transitions are well documented [55,56], and is consistent with the doming model previously proposed for interfluve pockmarks in the Gulf of Lions [41]. Following this hypothesis, three spatial scenarios can be identified in the Gulf of Lions (Fig. 6): (i) domes without Type B pockmarks on the shelf in the western sector, (ii) the co-occurrence of domes and Type B pockmarks on the shelf in the eastern sector, and (iii) Type B pockmarks without associated domes on the interfluves of the upper slope. This spatial distribution suggests that the Gulf of Lions displays different stages of morphological evolution across distinct areas. Although chronological constraints are not currently available, these observations imply that dome maturation and transition towards pockmark is a slow process involving different times, progress rates and sectors in the Gulf of Lions.

Type C pockmarks (Fig. 3-c) differ from Type A and B pockmarks by their small size (<15 m diameter) and very peculiar distribution, closely tied to the infralittoral prograding wedge (IPW), as defined by Hernandez-Molina et al. [52]. This geomorphological unit represents a reworked, storm-influenced wedge of material deposited in the infralittoral zone. Type C pockmarks are found at the top of the IPW (15 to 35 m water depth), possibly generated by ground-water expulsions. It may come either from water released during storm-induced remobilization of the IPW, or freshwater discharges from coastal aquifers, a well-known process documented on several sites in the Mediterranean shelves including the Gulf of Lions [57]. Seismic indicators typically associated to presence of gas, such as amplitude anomalies, gas masking, or polarity inversions are not observed in the Type C pockmarks, which favors the hypothesis of submarine ground-water discharge.

Type D pockmarks (Fig. 3-d) unlike others, display highly variable size and morphology, yet their water depth (70 to 100 m water depth) remains uniform across the study area. Their shape and size along with the absence of gas indicators suggest that these pockmarks may be relicts and are now primarily erosional features, reshaped by the action of hydrodynamic processes. This hypothesis is supported by the correlation with core MD99-2352 (Fig. 1-e and Fig. 9 in [35]) illustrating that these pockmarks are anchored on a coarse-grained shell lag corresponding to the MFS [46]. The grain-size contrast between the overlying fine-grained muds and the coarser deposits of the MFS might act as a mechanical an erosion-resistant barrier, preventing erosion of the underlying muds and explaining both the distinct flat-bottom shape of the pockmarks and the apparent influence of lithological variability revealed by the model. Pockmarks activity is closely related to the lithology of the sea floor, and can be highly responsive to hydrodynamic forcing [58,59], where bottom currents and/or wave-induced pressure variations promote sediment resuspension [60]. Such mechanisms could explain the morphological variability and diversity of observed shapes. Furthermore, the compound or irregular shape of depressions may suggest the coalescence of smaller Type D pockmarks.

The occurrence of **spiky pockmarks** (Fig. 3-e) above the Shoal Retreat Massifs (Fig. 6-a), such as the Early Rhône Deltaic Complex and Lacaze-Duthiers systems, suggests a strong genetic link with sandy sediment distributions, confirmed by the model. Unlike classical pockmarks, these structures are characterized by a central relief or “spike,” surrounded by a depression. Such morphologies may form where authigenic carbonate precipitates within sandy horizons, cementing sediment grains and producing a rigid central structure [61]. This

carbonate crust resists erosion and compaction, forming the spike on the seabed. In contrast, the surrounding unconsolidated sandy sediments undergo differential compaction and winnowing, generating a circular to elongated depression around the resistant carbonate spike. The resulting morphology is therefore the combined product of focused seepage, carbonate precipitation, and sedimentological contrasts. In the Gulf of Lions the spiked pockmarks develop exclusively where underlying sandy bodies are present and intersect fluid escape pathways. This might explain the formation of a carbonate-cemented spike that requires a sufficiently permeable sandy matrix to act as both a fluid conduit and a site for carbonate precipitation. This sedimentological model, which links the nature of sediments, geological processes, and the morphology of fluid escape structures, should be validated by field observations, which are not available yet.

VI. Conclusion

This study provides the first comprehensive inventory and quantitative characterization of sediment deformation structures in the Gulf of Lions. Through the integration of high-resolution bathymetric and seismic data with geostatistical and machine learning approaches, we demonstrate that pockmarks and domes, are widespread from the inner shelf to the continental slope. Both spatial mapping and machine-learning analysis reveal that their occurrence is not random but follows systematic patterns controlled primarily by sediment thickness, water depth, slope gradient, and grain-size distribution. These patterns, along with seismic interpretation, point to the key role of the Maximum Flooding Surface, the presence of subsurface sand bodies, and the overlying mud belt in modulating the distribution of pockmarks and domes across the shelf.

Within this framework, domes represent the most abundant structures. They are consistently associated with seismic anomalies correlated to gas trapping at the Maximum Flooding Surface, inside the mud belt. The most common type of pockmarks (Type B) frequently occur in association with domes, supporting an evolutionary pathway whereby dome growth transitions into collapse structures once mechanical thresholds are exceeded. Largest pockmarks (Type A), preferentially located on canyon interfluves, correspond to deep-rooted, gas-related structures influenced by cyclic sediment loading and fluid migration. In contrast, Type C, D, and spiky pockmarks develop in or above thinly draped sandy sediments.

While this study allows for a better understanding of the morphology and distribution of pockmarks and domes across the Gulf of Lions, formation processes remain uncertain. Type A and Type B pockmarks were already described as governed by fluid overpressure and stratigraphic sealing within fine-grained sediments. Domes are observed for the first time in the Gulf of Lions. Their morphology and the presence of seismic anomalies below domes suggest that doming is associated with fluids overpressure, similarly to what was observed in previous studies worldwide. On the other hand, the absence of seismic anomalies correlated with Type C and Type D pockmarks suggests that they are influenced by different fluids or hydrodynamic processes.

Future research should integrate geochemical, biological, and temporal monitoring approaches to determine the precise source, activity, composition, and environmental significance of pockmarks and domes in the Gulf of Lions.

VII. References

1. Van Rensbergen, P., Hillis, R. R., Maltman, A. J. & Morley, C. K. *Subsurface Sediment Mobilization*. vol. 216 (The Geological Society, London, 2003).
2. Andresen, K. J. Fluid flow features in hydrocarbon plumbing systems: What do they tell us about the basin evolution? *Marine Geology* **332–334**, 89–108 (2012).
3. Suess, E. Marine cold seeps and their manifestations: geological control, biogeochemical criteria and environmental conditions. *Int J Earth Sci (Geol Rundsch)* **103**, 1889–1916 (2014).
4. Gay, A. *et al.* Isolated seafloor pockmarks linked to BSRs, fluid chimneys, polygonal faults and stacked Oligocene–Miocene turbiditic palaeochannels in the Lower Congo Basin. *Marine Geology* **226**, 25–40 (2006).
5. Judd, A. & Hovland, M. *Seabed Fluid Flow: The Impact on Geology, Biology and the Marine Environment*. (Cambridge University Press, Cambridge, 2007). doi:10.1017/CBO9780511535918.
6. Vaknin, I., Aharonov, E., Holtzman, R. & Katz, O. Gas Seepage and Pockmark Formation From Subsurface Reservoirs: Insights From Table-Top Experiments. *Journal of Geophysical Research: Solid Earth* **129**, e2023JB028255 (2024).
7. Kvenvolden, K. A. Gas hydrates—geological perspective and global change. *Reviews of Geophysics* **31**, 173–187 (1993).
8. Whiticar, M. J. Carbon and hydrogen isotope systematics of bacterial formation and oxidation of methane. *Chemical Geology* **161**, 291–314 (1999).
9. Tissot, B. P. & Welte, D. H. *Petroleum Formation and Occurrence*. (Springer, Berlin, Heidelberg, 1984). doi:10.1007/978-3-642-87813-8.

10. King, L. H. & MacLean, B. Pockmarks on the Scotian Shelf. *GSA Bulletin* **81**, 3141–3148 (1970).
11. Pilcher, R. & Argent, J. Mega-pockmarks and linear pockmark trains on the West African continental margin. *Marine Geology* **244**, 15–32 (2007).
12. Spatola, D., Rovere, M., Casalbore, D. & Chiocci, F. L. Pockmarks of the Mediterranean region seas: A Comprehensive Geodatabase for Marine Geomorphological Analysis. *Sci Data* **12**, 1049 (2025).
13. León, R. *et al.* Pockmarks on either side of the Strait of Gibraltar: formation from overpressured shallow contourite gas reservoirs and internal wave action during the last glacial sea-level lowstand? *Geo-Mar Lett* **34**, 131–151 (2014).
14. Barry, M., Boudreau, B. & Johnson, B. Gas domes in soft cohesive sediments. *Geology* **40**, 379–382 (2012).
15. Diercks, A.-R. *et al.* High-resolution seismo-acoustic characterization of Green Canyon 600, a perennial hydrocarbon seep in Gulf of Mexico deep water. *Mar Geophys Res* **40**, 357–370 (2019).
16. Hovland, M. & Judd, A. G. The global production of methane from shallow submarine sources. *Continental Shelf Research* **12**, 1231–1238 (1992).
17. Napoli, S. *et al.* Comprehensive global inventory of submarine mud volcanoes. *Sci Data* **12**, 382 (2025).
18. Naudts, L. *et al.* Geological and morphological setting of 2778 methane seeps in the Dnepr paleo-delta, northwestern Black Sea. *Marine Geology* **227**, 177–199 (2006).
19. Rise, L., Bellec, V. K., Chand, S. & Bøe, R. Pockmarks in the southwestern Barents Sea and Finnmark fjords. https://nynjg.geologi.no/publications/pockmarks-in-the-southwestern-barents-sea-and-finnmark-fjords/ (2014).

20. Cartwright, J., Huuse, M. & Aplin, A. Seal bypass systems. *AAPG Bulletin* **91**, 1141–1166 (2007).
21. Garcia-Garcia, A. *et al.* Shallow gas off the Rhone prodelta, Gulf of Lions. *Marine Geology* **234**, 215–231 (2006).
22. Mascle, A., Vially, R., Deville, E., Biju-Duval, B. & Roy, J. P. The petroleum evaluation of a tectonically complex area: The western margin of the Southeast Basin (France). *Marine and Petroleum Geology* **13**, 941–961 (1996).
23. Lofi, J., Berné, S., Tesson, M., Seranne, M. & Pezard, P. Giant solution-subsidence structure in the Western Mediterranean related to deep substratum dissolution. *Terra Nova* **24**, 181–188 (2012).
24. Widhen, F. *et al.* Long-term evolution of a carbonate reservoir submitted to fresh, saline and thermal waters interactions – Jurassic carbonates in the coastal area of the Gulf of Lion margin (southern France). *Bulletin de la Société Géologique de France* **194**, 7 (2023).
25. Baztan, J. *et al.* Axial incision: The key to understand submarine canyon evolution (in the western Gulf of Lion). *Marine and Petroleum Geology* **22**, 805–826 (2005).
26. Lofi, J. *et al.* Plio-Quaternary prograding clinoform wedges of the western Gulf of Lion continental margin (NW Mediterranean) after the Messinian Salinity Crisis. *Marine Geology* **198**, 289–317 (2003).
27. Rabineau, M. *et al.* Paleo sea levels reconsidered from direct observation of paleoshoreline position during Glacial Maxima (for the last 500,000 yr). *Earth and Planetary Science Letters* **252**, 119–137 (2006).
28. Bassetti, M. A. *et al.* The 100-ka and rapid sea level changes recorded by prograding shelf sand bodies in the Gulf of Lions (western Mediterranean Sea). *Geochem. Geophys. Geosyst.* **9**, (2008).

29. Bassetti, M. A. *et al.* Sand bodies at the shelf edge in the Gulf of Lions (Western Mediterranean): Deglacial history and modern processes. *Marine Geology* **234**, 93–109 (2006).
30. Tesson, M. *et al.* Quaternary “Compound” Incised Valley In A Microtidal Environment, Roussillon Continental Shelf, Western Gulf of Lions, France. *Journal of Sedimentary Research* **81**, 708–729 (2011).
31. Berné, S. *et al.* A “natural sand plant” at the shelf edge in the low-energy Gulf of Lions, western Mediterranean Sea. *Geology* **52**, 911–916 (2024).
32. Berné, S., Lericolais, G., Marsset, T., Bourillet, J. F. & de Batist, M. Erosional shelf sand ridges and lowstand shorefaces: examples from tide and wave dominated environments of France. *Journal of Sedimentary Research* **68**, 540–555 (1998).
33. Swift, D. J. P. Delaware Shelf Valley: estuary retreat path, not drowned river valley. *Geological Society of America Bulletin* **84**, 2743–2748 (1973).
34. Swift, D. J. P., Sears, P. C., Bohlke, B. & Hunt, R. Evolution of a shoal retreat massif, North Carolina Shelf: Inferences from areal geology. *Marine Geology* **27**, 19–42 (1978).
35. Berné, S., Jouet, G., Bassetti, M. A., Dennielou, B. & Taviani, M. Late Glacial to Preboreal sea-level rise recorded by the Rhone deltaic system (NW Mediterranean). *Marine Geology* **245**, 65–88 (2007).
36. Bassetti, M. A. *et al.* Holocene hydrological changes in the Rhône River (NW Mediterranean) as recorded in the marine mud belt. *Clim. Past* **12**, 1539–1553 (2016).
37. Zecchin, M., Catuneanu, O. & Caffau, M. High-resolution sequence stratigraphy of clastic shelves IX: Methods for recognizing maximum flooding conditions in shallow-marine settings. *Marine and Petroleum Geology* **156**, 106468 (2023).

38. Aloïsi, J. C. Sur un modèle de sédimentation deltaïque: contribution à la connaissance des marges passives. (1986).
39. Bourrin, F. Variabilité et devenir des apports sédimentaires par les fleuves côtiers : cas du système Têt-littoral roussillonnais dans le golfe du Lion. (Perpignan, 2007).
40. Piégay, H. *et al. OSR - Observatoire Des Sédiments Du Rhône. 12 Années de Recherche Pour La Connaissance et La Gestion Hydro-Sédimentaire Du Fleuve. Bilans et Perspectives Scientifiques*. https://archimer.ifremer.fr/doc/00808/92047/ (2022).
41. Gay, A., Cavailhès, T., Grauls, D., Marsset, B. & Marsset, T. Repeated fluid expulsions during events of rapid sea-level rise in the Gulf of Lion, western Mediterranean Sea. *Bulletin de la Société Géologique de France* **188**, 24 (2017).
42. Riboulot, V., Thomas, Y., Berné, S., Jouet, G. & Cattaneo, A. Control of Quaternary sea-level changes on gas seeps. *Geophysical Research Letters* **41**, 4970–4977 (2014).
43. Krämer, K. *et al.* Abrupt emergence of a large pockmark field in the German Bight, southeastern North Sea. *Sci Rep* **7**, 5150 (2017).
44. Conrad, O. *et al.* System for Automated Geoscientific Analyses (SAGA) v. 2.1.4. *Geoscientific Model Development* **8**, 1991–2007 (2015).
45. Uber Technologies. Uber's H3 Hexagonal Hierarchical Geospatial Indexing System. *Github* https://github.com/uber/h3 (2023).
46. Jouet, G. Enregistrements stratigraphiques des cycles climatiques et glacio-eustatiques du Quaternaire terminal. Modélisations de la marge continentale du Golfe du Lion. (Université de Bretagne Occidentale, 2007).

47. EMODnet Bathymetry Consortium. EMODnet Digital Bathymetry (DTM 2024). EMODnet Bathymetry Consortium https://doi.org/10.12770/CF51DF64-56F9-4A99-B1AA-36B8D7B743A1 (2024).
48. Augris, C. *et al.* Seabed substrate database from a compilation of sediment samples taken during oceanographic campaigns carried out in the Gulf of Lion by Ifremer, CEFREM, IRSN, CEREGE, FOB, MIO, LECOB, The Conseil Général de l'Hérault and Rhône-Méditerranée-Corse Water Agency. Results of grain size analysis performed on samples. SEANOE https://doi.org/10.17882/81430 (2013).
49. Y. Shi *et al.* Light Gradient Boosting Machine. Microsoft (2025).
50. Lundberg, S. & Lee, S.-I. A Unified Approach to Interpreting Model Predictions. Preprint at https://doi.org/10.48550/arXiv.1705.07874 (2017).
51. Taner, M. T. & Sheriff, R. E. Application of Amplitude, Frequency, and Other Attributes to Stratigraphic and Hydrocarbon Determination: Section 2. Application of Seismic Reflection Configuration to Stratigraphic Interpretation. in (1977).
52. Hernandez-Molina, F. J. *et al.* The infralittoral prograding wedge: a new large-scale progradational sedimentary body in shallow water environments. *Geo-Marine Letters* **20**, 109–117 (2000).
53. Brooke, C. M., Trimble, T. J. & Mackay, T. A. Mounded shallow gas sands from the Quaternary of the North Sea: analogues for the formation of sand mounds in deep water Tertiary sediments? *SP* **94**, 95–101 (1995).
54. Cathles, L. M., Su, Z. & Chen, D. The physics of gas chimney and pockmark formation, with implications for assessment of seafloor hazards and gas sequestration. *Marine and Petroleum Geology* **27**, 82–91 (2010).
55. Koch, S. *et al.* Gas-controlled seafloor doming. *Geology* **43**, 571–574 (2015).

56. Loher, M. *et al.* Seafloor sealing, doming, and collapse associated with gas seeps and authigenic carbonate structures at Venere mud volcano, Central Mediterranean. *Deep Sea Research Part I: Oceanographic Research Papers* **137**, 76–96 (2018).

57. Ollivier, P., Claude, C., Radakovitch, O. & Hamelin, B. TIMS measurements of 226Ra and 228Ra in the Gulf of Lion, an attempt to quantify submarine groundwater discharge. *Marine Chemistry* **109**, 337–354 (2008).

58. Schattner, U., Lazar, M., Souza, L. A. P., ten Brink, U. & Mahiques, M. M. Pockmark asymmetry and seafloor currents in the Santos Basin offshore Brazil. *Geo-Mar Lett* **36**, 457–464 (2016).

59. Böttner, C. *et al.* The Enigmatic Pockmarks of the Sandy Southeastern North Sea. *Geochemistry, Geophysics, Geosystems* **25**, e2024GC011837 (2024).

60. Pau, M., Gisler, G. & Hammer, Ø. Experimental investigation of the hydrodynamics in pockmarks using particle tracking velocimetry. *Geo-Mar Lett* **34**, 11–19 (2014).

61. Coughlan, M. *et al.* Geological settings and controls of fluid migration and associated seafloor seepage features in the north Irish Sea. *Marine and Petroleum Geology* **123**, 104762 (2021).

Acknowledgements

We thank OFB (notably Grégory Agin), IFREMER (Gwénaël Jouet), Shom (Yann Le Faou), RTE (Jules Lacombe), EDF (Thierry Denois), DGEC (Guillaume Poirier) and Engie (Samuel Lemière) for providing access to data, as well as Genavir and Technoambiente teams for data acquisition. Additional seismic data were acquired by the DEM'EAUX project, funded by the French Government, Région Occitanie, Agence de l'Eau, Perpignan Métropôle and département des Pyrénées Orientales. We are grateful to Marina Rabineau and Estelle Leroux for access to the AMMED cruise dataset, and to Olivier Raynal and Bertil Hébert (CEFREM) for their participation in data acquisition. We also thank Lies Loncke (CEFREM) for valuable suggestions.

Contributions

AL contributed to conceptualization, data analysis, interpretation and writing. SB contributed to conceptualization, data acquisition and analysis, interpretation and writing. MAB contributed to conceptualization, interpretation and writing. RJ contributed to conceptualization, interpretation and writing.

Corresponding author

Correspondence to André Lion

Data availability statement

Geophysical data: The raw public data, acquired by IFREMER vessels, are openly available on the SISMER website at [https://data.ifremer.fr/#/home].

Other raw geophysical data that support the findings of this study are available upon request to MAB with the permission of third party owners (see Supplementary table 1).

The surface sedimentological data that support the findings of this study are openly available on SEANOE website at [https://doi.org/10.17882/81430].

The interpretations that support the findings of this study are available from the corresponding author, AL, upon reasonable request.

Competing interests

The author(s) declare no competing interests

Research funding

This research did receive funding.

André Lion received funding from French Ministry of Higher Education, Research and Space.

André Lion received funding from Office Français de la Biodiversité.

Figures and Tables

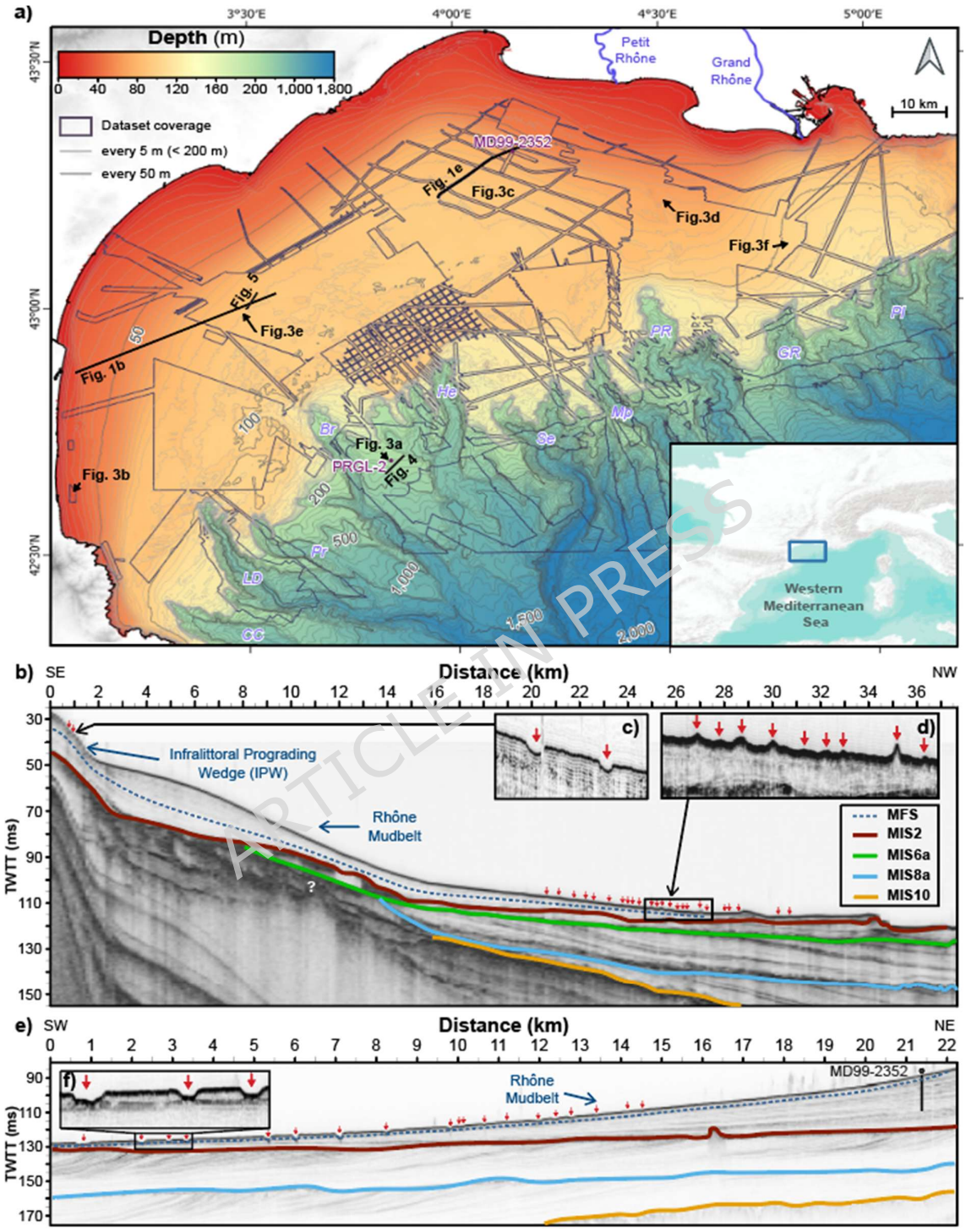

*Figure 1: **(A)** General bathymetric map of the Gulf of Lions. Dark-blue line represents DEM dataset coverage. Isobath contour-line interval is 5m from 0 to 200 m water depth, 50 m beyond 200 m; **(B)** Interpreted seismic (chirp) section across the western Gulf of Lions continental shelf (position in Fig. **Error! Reference source not found.**-a); **(C)** Closeup view of seafloor deformation structures (SDS) – Type C pockmarks; **(D)** Closeup view of SDS –*

*Domes; (**E**) Interpreted seismic (chirp) section across the eastern Gulf of Lions continental shelf (position in Fig. **Error! Reference source not found.**-a); (**F**) Closeup view of SDS – Type D pockmarks. SDS are indicated by red arrows. For simplicity, seismic bounding surfaces are assigned to the Marine Isotope Stages ending the periods of sea-level fall (at the top of the falling stage systems tracts). The chronology is based on stratigraphic correlations from the nearby PRGL-2 drillsite* [28]*. Uninterpreted seismic sections are available in supplementary figure 1.*

CC = Cap de Creus Canyon; LD = Lacaze-Duthiers Canyon; Br = Bourcart Canyon; He = Hérault Canyon; Se = Sète Canyon; Mp = Montpellier Canyon; PR = Petit Rhone Canyon; GR = Grand Rhone Canyon; Pl = Planier Canyon

a)

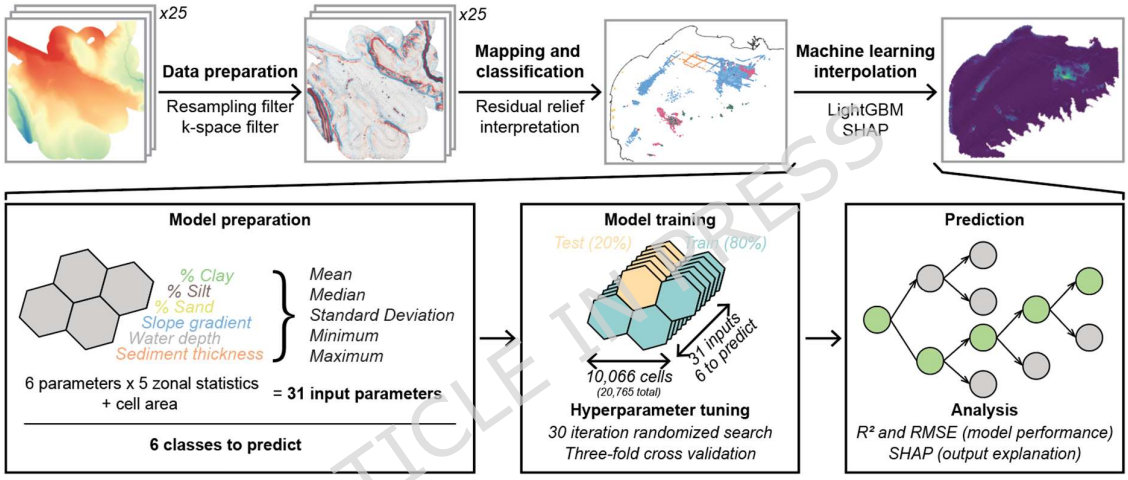

b)

	Train		Test	
Type	R^2	RMSE	R^2	RMSE
Domes	0.99	0.89	0.80	4.75
Pockmark Type A	0.55	0.26	0.33	0.43
Pockmark Type B	0.89	0.74	0.66	1.40
Pockmark Type C	0.93	0.19	0.42	1.30
Pockmark Type D	0.83	0.11	0.50	0.20
Spiky Pockmarks	0.25	0.03	0.02	0.05

Figure 2: (A) Visual workflow of data processing, mapping and modelling steps; (B) Performance metrics of the machine-learning model (R^2 and RMSE) for training and testing subsets by class

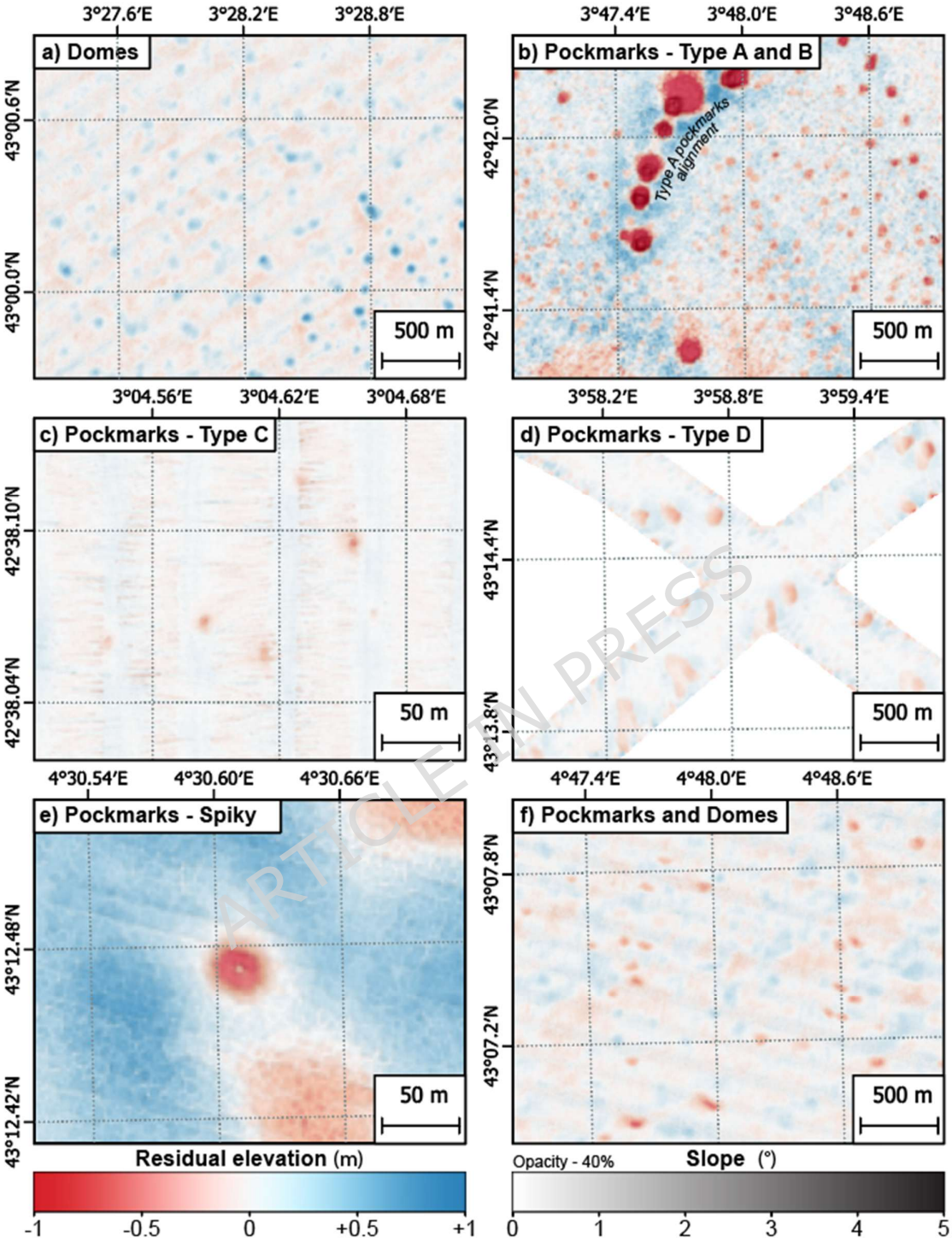

*Figure 3: Residual elevation maps of the six types of seafloor deformations found in the Gulf of Lions, shaded with slope gradient at 40 percent opacity: **(A)** Type A alignment in a Type B pockmark field on the upper continental slope (350-m water depth); **(B)** Domes field (85-m water depth); **(C)** Type C pockmarks cluster, (25-m water depth); **(D)** Type D pockmarks field (75-m water depth); **(E)** Isolated spiky pockmarks (85-m water depth); **(F)** Type B pockmarks and domes association (100-m water depth). Color scales for both residual elevation and slope gradient are common to all closeups.*

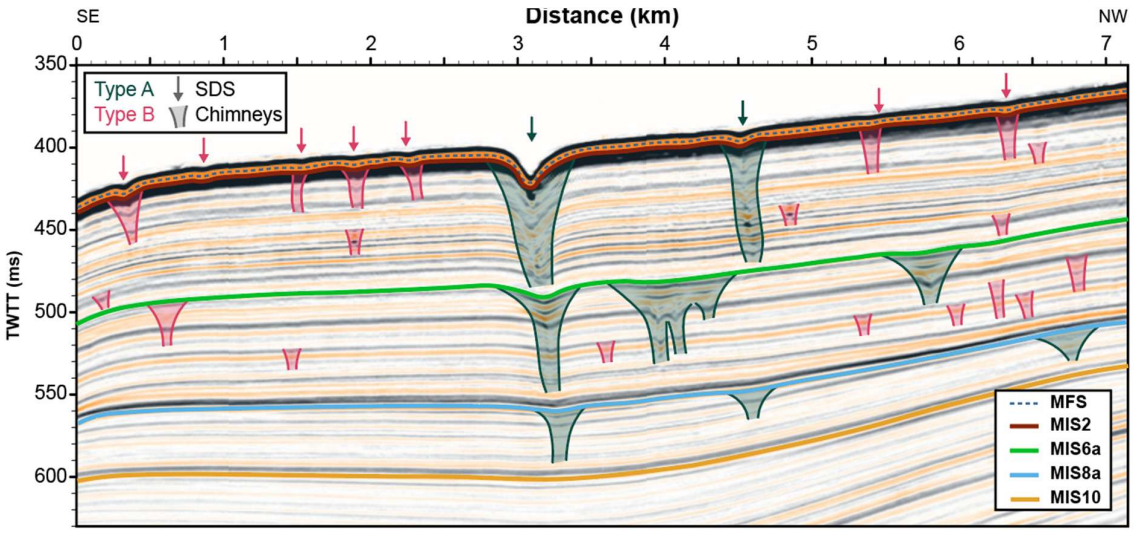

Figure 4: Interpreted seismic (3D sparker) section across the Bourcart-Hérault canyon interfluve, upper continental slope of the Gulf of (position in Fig. ***Error! Reference source not found.****-a); The identification of major seismic surfaces (correlative conformities of shelf sequence boundaries) is based on stratigraphic correlations from the nearby PRGL-2 drillsite* [28]. *Surface Deformation Structures (SDS) are reported on seismic section from residual bathymetry. Uninterpreted seismic section is available in supplementary figure 1.*

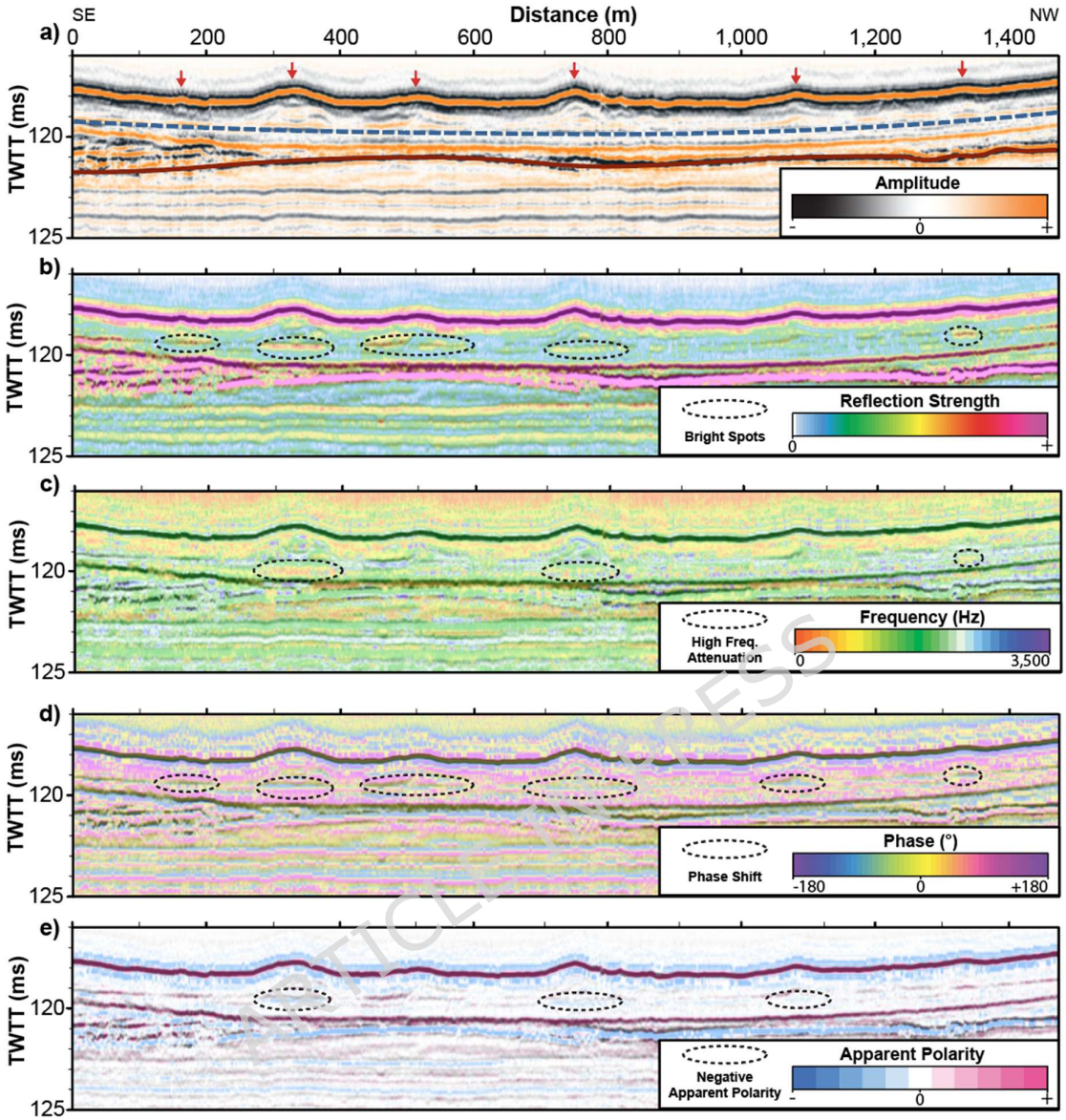

*Figure 5: Instantaneous seismic attributes computed on seismic data overlapped on seismic (sparker) section across a dome field (individual domes indicated by red arrows): **(A)** Original – Amplitude, blue dotted line is the Maximum Flooding Surface (MFS), correlated from Bassetti et al.* [36]; *(B) Reflection Strength; **(C)** Instantaneous Frequency; **(D)** Instantaneous Phase; **(E)** Apparent Polarity (signal polarity at maximum reflection strength). Attributes computation and color palettes follow SEG guidelines from Taner and Sheriff* [51]. Position in Figure 1-a.

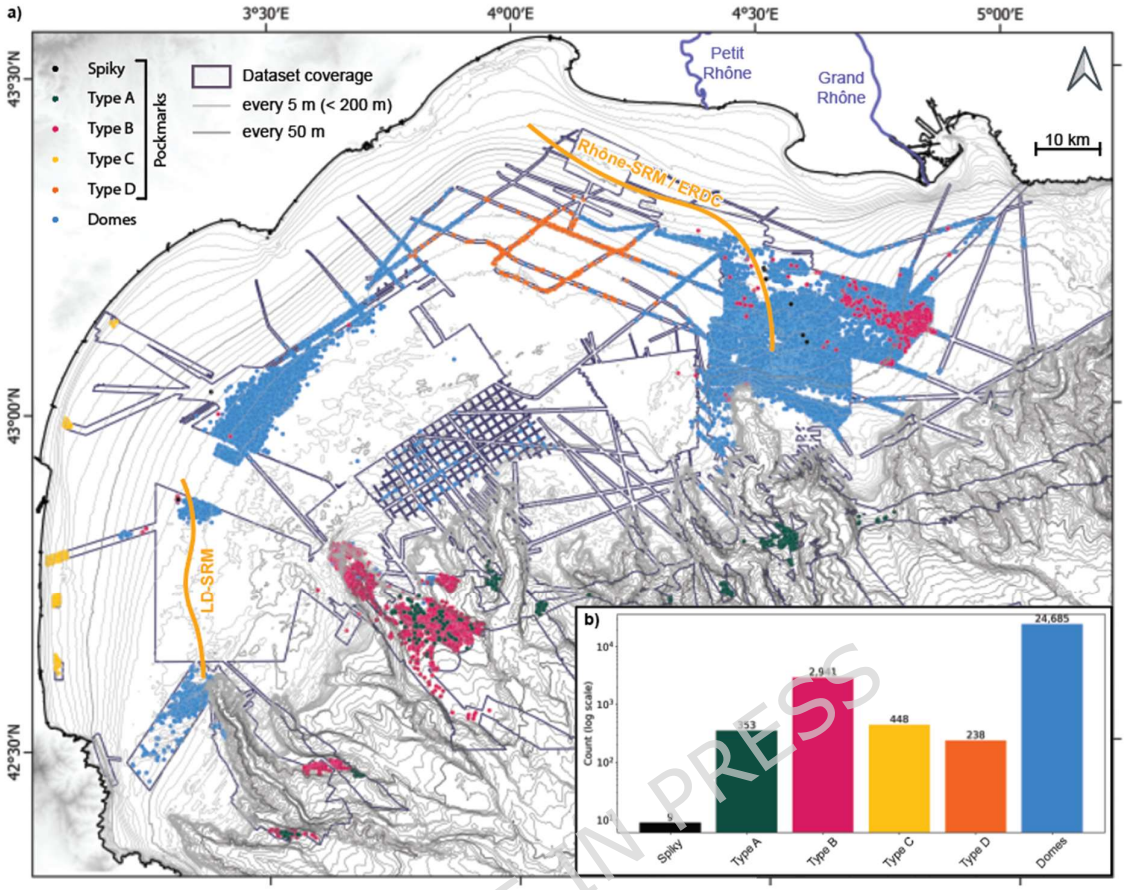

Figure 6: ***(a)*** *Map of the manually interpreted seafloor deformations structures (SDS). The dark-blue line represents the envelope of the DEM dataset. Isobath contour line interval is 5 m from 0 to 200 m water depth, 50 m beyond 200 m. Rhône-SRM / ERDC = Rhône Shoal Retreat Massif and Early Rhône Deltaic Complex; LD-SRM = Lacaze-Duthiers Shoal Retreat Massif,* ***(b)*** *Distribution of SDS types (logarithmic scale)*

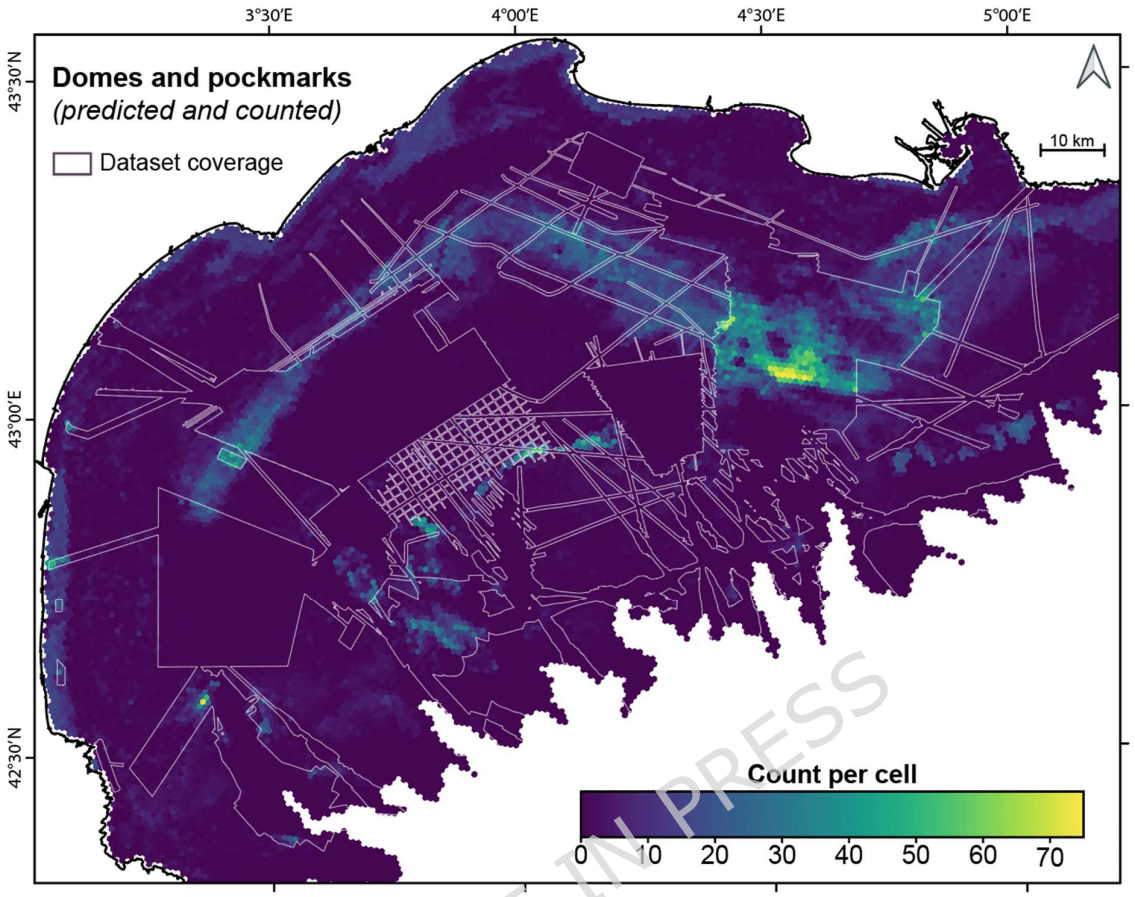

Figure 7: Machine learning (LightGBM) prediction of counts of seafloor deformations per H3 Grid cell. The map represents both predicted and manually counted pockmarks and domes. *White line represents the envelope of DEM dataset coverage. Results for individual classes are found in supplementary figure 3.*

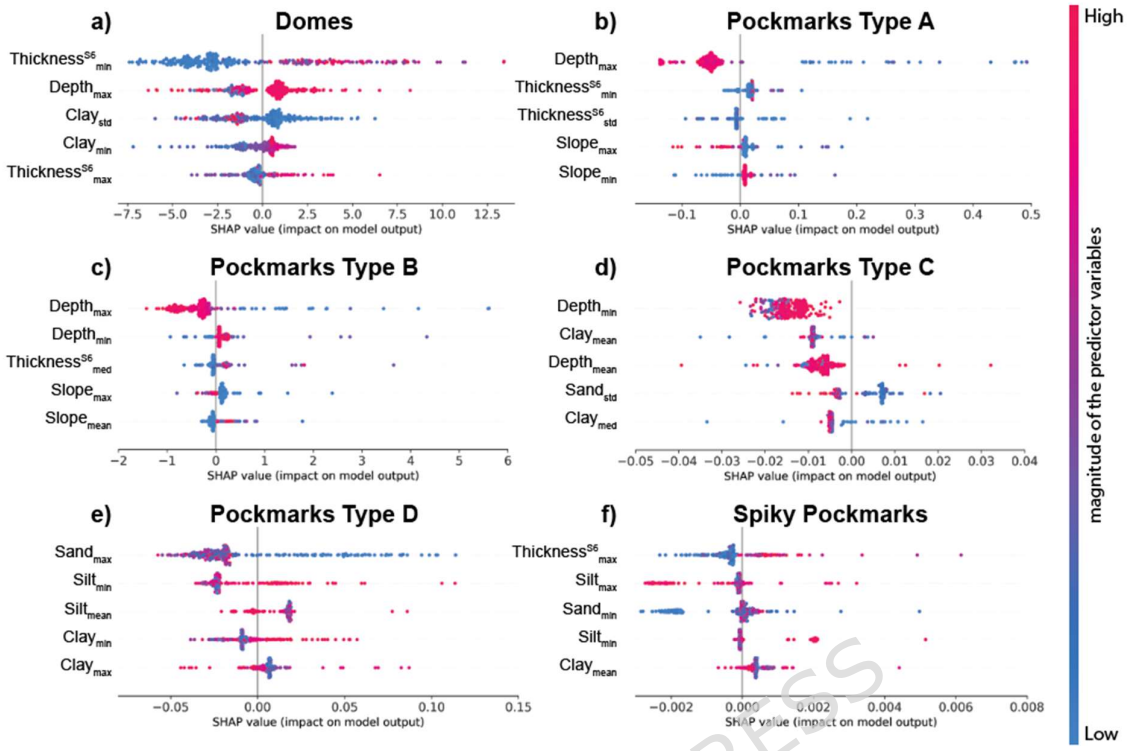

*Figure 8: Individual SHAP summary plots for the 5 most influential predictor variables used by the model for each type: (**A**) Domes; (**B**) Type A pockmarks; (**C**) Type B pockmarks; (**D**) Type C pockmarks; (**E**) Type D pockmarks; (**F**) Spiky pockmarks. Predictive variables are ranked (top to bottom) by their contribution to the model prediction; the position of the point on horizontal axis indicates the direction and amplitude of the variable impact on the model (0 = no impact); the color of individual points represents the magnitude of the corresponding predictor variable. Depth in the model is expressed as elevation below sea level (negative values), this causes an inversion when reading magnitude for depth: blue dots (low values) represent deeper depths)*

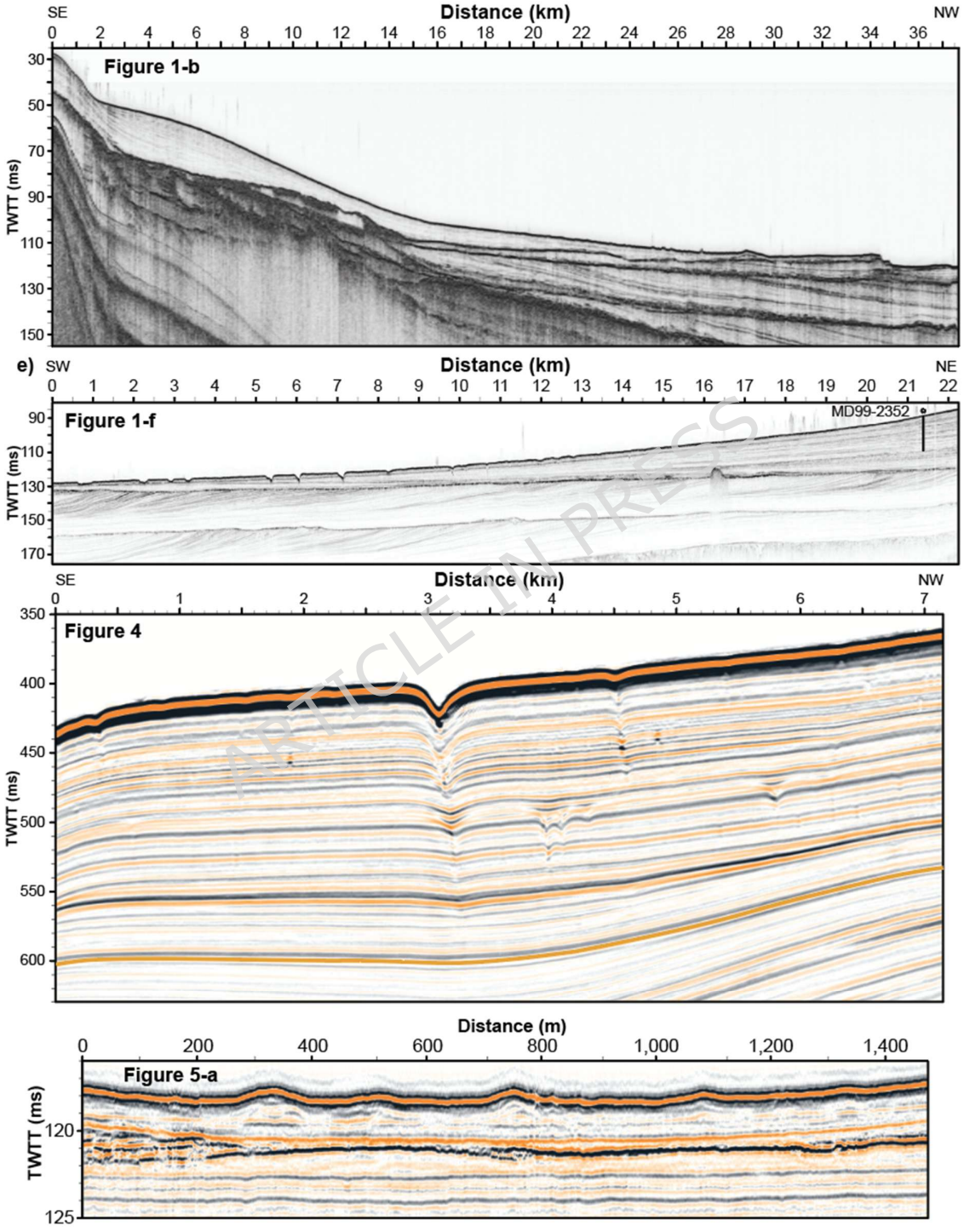

Supplementary Figure 1: Uninterpreted seismic sections, numbers on the panels correspond to the interpreted seismic sections in the article.

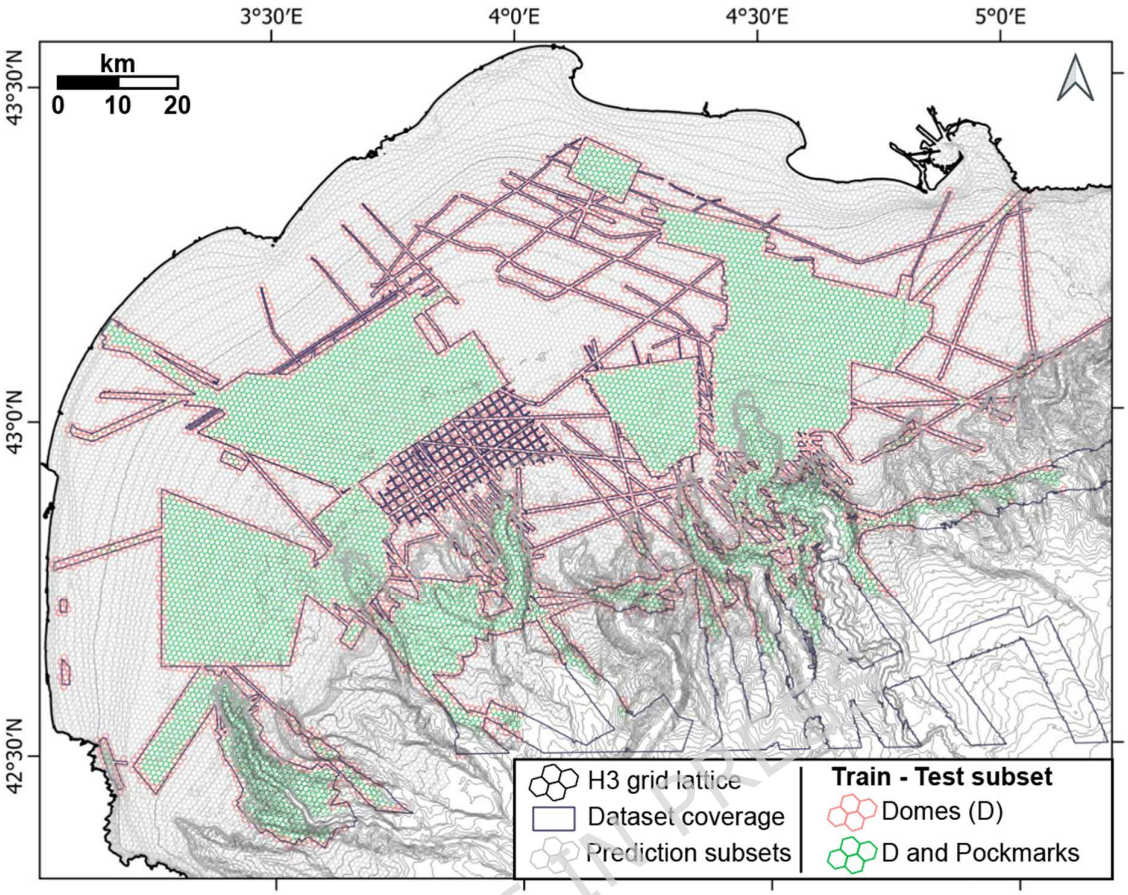

Supplementary Figure 2: Dataset coverage (merge of all Digital Depth Models) and H3 Grid used for machine learning. The pool of cells used in the machine learning train and test subsets is represented in color (red and green). Green cells were used to predict domes and pockmarks; Red cells were added to the subset for pockmarks only. Isobath contour-line interval is 5m from 0- to 200-m water depth, 50 m beyond 200 m.

Supplementary Table *1: Digital Depth Models used in this study, with their associated metadata. MBES = Multibeam echosounder. Note that surface overlaps have been subtracted.*

Cruise - Identifier	Year	Horizontal resolution (m)	Surface (km²)	MBES model	Owner(s)
AMMED 1 – Leg 1	2013	10	2254	EM302	IFREMER
AMMED 1 – Leg 2	2013	10		EM302	IFREMER
Basar 2 – Aude	1995	10	112	EM950	IFREMER
Caladu	2021	10	291	EM304	IFREMER
Caladu - Transit	2021	20	579	EM304	IFREMER
Calimero 1 – A	2004	10	88	EM300	IFREMER - Shom
Calimero 1 – B	2004	10	74	EM300	IFREMER - Shom
Calimero 2	2005	10	210	EM300	IFREMER - Shom
Calmar99 – Aude	1999	10	47	EM1000	IFREMER
Cartham 1 - South	*2010*	1	107	R2Sonic 2024	OFB
Corridor A	2022	1	20	EM712	DGEC – RTE
Corridor B	2022	1	53	EM712	DGEC – RTE
Corridor D	2022	1	11	EM712	DGEC – RTE
Corridor PGL	2013	2	12	N/A	EDF
Famosa – Z1	2024	1	8	EM2040	OFB
Famosa – Z2	2024	1	12	EM2040	OFB
Famosa – Z3	2024	1	10	EM2040	OFB
OWF AO6 – ZA	2021	1	583	EM712	DGEC
OWF AO6 – ZB	2021	1	869	EM712	DGEC
OWF AO6 – ZC	2023	3	258	EM712	DGEC
OWF AO6 – ZD	2021	1	574	EM712	DGEC
OWF AO10	2024	1	73	EM712	DGEC
RefMed – Canet	2016	0.5	2	R2Sonic 2024	OFB
RefMed – StCyp	2016	0.5	4	R2Sonic 2024	OFB
Rhosos – ERDC	2008	5	377	EM300	IFREMER/UPVD
Rhosos – Béar	2008	5	13	EM300	IFREMER/UPVD

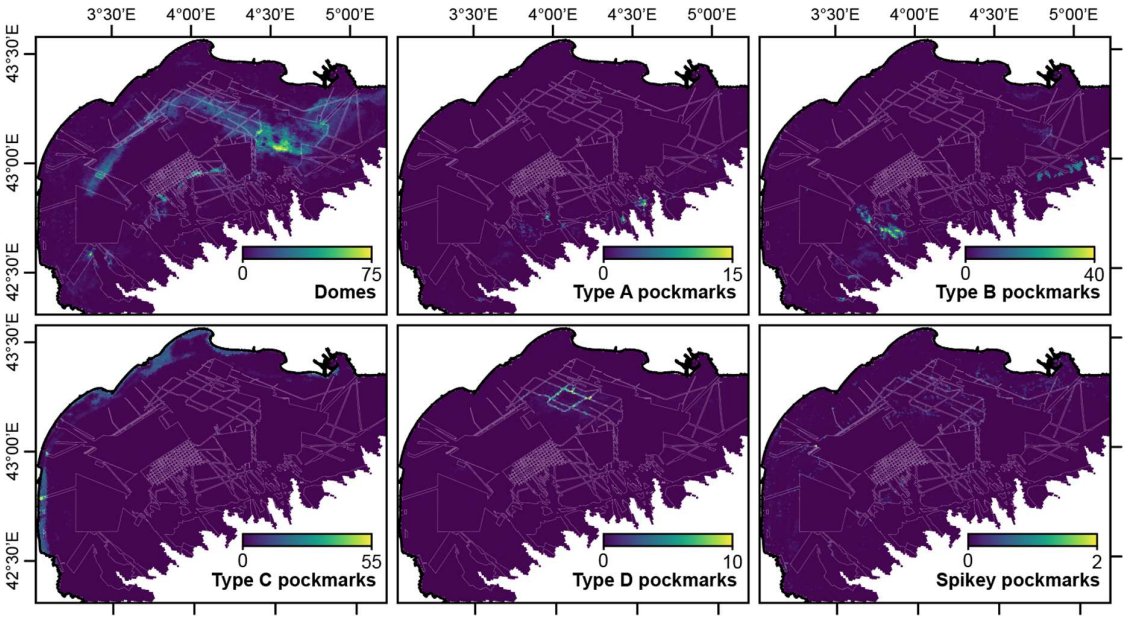

Supplementary figure 3: Machine learning (LightGBM) predictions on counts of seafloor deformations per H3 Grid cell: Predicted and manually counted results for individual classes.